

Sparsity regularization for inverse problems with nullspaces

Ole Løseth Elvetun* and Bjørn Fredrik Nielsen†

May 17, 2022

Abstract

We study a weighted ℓ^1 -regularization technique for solving inverse problems when the forward operator has a significant nullspace. In particular, we prove that a sparse source can be exactly recovered as the regularization parameter α tends to zero. Furthermore, for positive values of α , we show that the regularized inverse solution equals the true source multiplied by a scalar γ , where $\gamma = 1 - c\alpha$. Our analysis is supported by numerical experiments for cases with one and several local sources.

This investigation is motivated by PDE-constrained optimization problems arising in connection with ECG and EEG recordings, but the theory is developed in terms of Euclidean spaces. Our results can therefore be applied to many problems.

1 Introduction

Consider the challenge of identifying a sparse source in an elliptic PDE from Dirichlet boundary data:

$$\min_{(f,u) \in F_h \times H^1(\Omega)} \left\{ \frac{1}{2} \|u - d\|_{L^2(\partial\Omega)}^2 + \alpha \|Wf\|_{L^1(\Omega)} \right\} \quad (1)$$

subject to

$$\begin{aligned} -\Delta u + \epsilon u &= f \quad \text{in } \Omega, \\ \frac{\partial u}{\partial \mathbf{n}} &= 0 \quad \text{on } \partial\Omega, \end{aligned} \quad (2)$$

where we employ weighted L^1 -regularization in (1). Here, F_h is a finite-dimensional subspace of $L^2(\Omega)$, $W : F_h \rightarrow F_h$ is a linear regularization operator, $\alpha > 0$ is a

*Faculty of Science and Technology, Norwegian University of Life Sciences, P.O. Box 5003, NO-1432 Ås, Norway. Email: ole.elvetun@nmbu.no.

†Faculty of Science and Technology, Norwegian University of Life Sciences, P.O. Box 5003, NO-1432 Ås, Norway. Email: bjorn.f.nielsen@nmbu.no. Nielsen's work was supported by The Research Council of Norway, project number 239070.

regularization parameter, d represents the Dirichlet boundary data, ϵ is a parameter, \mathbf{n} denotes the outwards pointing unit normal vector of the boundary $\partial\Omega$ of the bounded domain Ω , and f is the unknown source.

Variants of this inverse source problem appear in many applications, such as in crack determination, in the inverse ECG problem and in electroencephalography (EEG). Consequently, it has received much attention from researchers, see, e.g., [1, 2, 6, 9, 19, 21, 22, 23, 25, 31, 33]. However, in these studies the authors did not use ℓ^1 -regularization. A more detailed description of previous investigations is presented in [10].

Regularization of inverse problems with sparsity promoting methods has increased in popularity in recent years [7, 16, 27, 12]. In this context, the notion of sparsity, with respect to a given basis $\{\phi_i\}$ for the control space, means that the inverse solution f^* can be represented using very few of the basis functions. That is, if we expand the inverse solution f^* as $f^* = \sum_i f_i \phi_i$, then $f_i = (f^*, \phi_i) \neq 0$ only for very few of the basis functions. If we have s such non-zero components, we say that the solution f^* is s -sparse.

In *compressed sensing* the study of ℓ^1 -regularization for the exact recovery of a sparse source from noise free data has been studied in detail [3, 4, 8]. To elaborate the main findings in [4], let us assume that \mathbf{A} is a matrix with a significant nullspace. If \mathbf{b}^\dagger is generated from a sparse source \mathbf{x}^\dagger , i.e., $\mathbf{b}^\dagger = \mathbf{A}\mathbf{x}^\dagger$, then the minimizer of

$$\min_{\mathbf{x} \in \mathbb{R}^n} \|\mathbf{x}\|_1 \quad \text{subject to} \quad \mathbf{A}\mathbf{x} = \mathbf{b}^\dagger,$$

is the true sparse solution \mathbf{x}^\dagger when a certain assumption, known as the *restricted isometry property*, is fulfilled.

In [17] the authors unified this result with the theory developed by the inverse problem community. In particular, they showed that the commonly used range condition, combined with an additional restricted injectivity condition on the forward operator, are weaker assumptions than the previously mentioned *restricted isometry property*, and they proved that the former conditions are the weakest which admit linear convergence rates for the regularized problem

$$\min_{\mathbf{x} \in \mathbb{R}^n} \left\{ \frac{1}{2} \|\mathbf{A}\mathbf{x} - \mathbf{b}\|_2^2 + \alpha \|\mathbf{x}\|_1 \right\}.$$

That is, for every $C > 0$, there exists $c > 0$ such that one of the solutions \mathbf{x}_α of the problem above satisfies

$$\|\mathbf{x}_\alpha - \mathbf{x}^\dagger\| \leq c\zeta$$

when the noise level is such that $\|\mathbf{b} - \mathbf{b}^\dagger\| = \|\mathbf{b} - \mathbf{A}\mathbf{x}^\dagger\| \leq \zeta$ and $\alpha = C\zeta$.

Numerical experiments indicate that the identification criteria, mentioned in the previous paragraph, are not fulfilled by the linear system associated with (1)-(2) when $\mathbf{W} = \mathbf{I}$ (the identity map), see Figure 1. This is the main motive for the present study.

Many researchers have explored the use of sparsity regularization in connection with PDEs, see, e.g., [15, 5, 20, 37, 26, 24, 28, 13, 35]. However, as far as

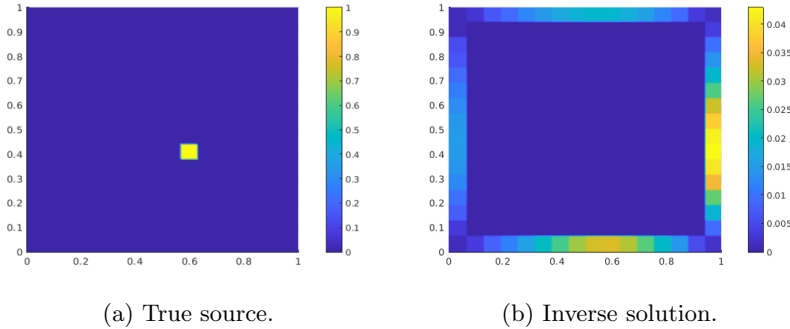


Figure 1: Panel (b) shows the outcome of attempting to use (1)-(2), with $W = I$ and $\alpha = 10^{-4}$, to recover the true source depicted in panel (a). That is, the Dirichlet boundary data d in (1) was generated by the true source (a).

the authors know, the use of weighted ℓ^1 -regularization to solve inverse source problems for PDEs, involving significant nullspaces, has not previously been attempted. We will therefore start with a brief motivation for developing sparsity promoting regularization for such problems in Section 2, before we in Section 3 prove that our methodology can recover, without any errors or blurring, a single local source. We also analyze a problem for which it is impossible to recover two separate sources. This implies that we can not guarantee, in general, that our approach can recover multiple local sources. However, in Section 4 many numerical experiments are presented, for both single and multiple sources, and we observe that several sources often can be successfully recovered.

We would like to emphasize that, even though our motivation originates from inverse source problems for elliptic PDEs, the general theory presented in this paper is applicable to any linear finite-dimensional inverse problem where the forward operator has a non-trivial nullspace.

2 Motivation

The purpose of EEG is to recover electrical activity in the brain from voltage recordings on the scalp. If one suspects that the true signal is spatially local, e.g., for focal epileptic seizures, it is natural to search for sparse solutions.

Similarly, in the inverse problem of ECG, the aim can be to locate an ischemic¹ region of the heart. This area will have an electrical potential which is different from the voltage in healthy tissue. The difference in the potential can be interpreted as the source in an elliptic PDE. If we assume that the ischemic region is small, with a sharp transition between ischemic and healthy tissue, it is reasonable to search for a sparse inverse solution.

The optimization problem which must be solved in connection with EEG

¹Ischemia is a precursor of a heart infarct.

and ECG recordings differs slightly from (1)-(2):

$$\min_{(f,u) \in F_h \times H^1(\Omega)} \left\{ \frac{1}{2} \sum_{i=1}^m (u_i - d_i)^2 + \alpha \|Wf\|_{L^1(\Omega)} \right\} \quad (3)$$

subject to

$$\begin{aligned} -\nabla \cdot (\sigma \nabla u) &= \underbrace{f}_{=\nabla \cdot \mathbf{j}^p} \quad \text{in } \Omega, \\ \frac{\partial u}{\partial \mathbf{n}} &= 0 \quad \text{on } \partial\Omega, \end{aligned} \quad (4)$$

where we, as above, employ weighted L^1 -regularization. Here, u_i and d_i denote the simulated and recorded electrical potentials at the position of electrode number i , respectively, $\sigma = \sigma(x)$ is a conductivity tensor [36, 29], and \mathbf{j}^p denotes the primary or impressed current. See, e.g., [34, 30, 32, 18] for further details. The lack of the zero order term ϵu in (4), compared to (2), implies that the solution of (4) is not unique. It is only determined up to a constant, but this matter can be handled by the techniques described in the appendix of [11]. (We also mention that (3)-(4) differs significantly from the inverse ECG problem which seeks to estimate the electrical potential at the heart surface from body surface measurements [13, 35]. The latter problem typically does not have a significant nullspace because it is closely related to the Cauchy problem for Laplace's equation.)

After discretization, both (1)-(2) and (3)-(4) can be formulated in terms of the so-called *transfer matrix* \mathbf{A} , which maps discrete versions of f to (u_1, u_2, \dots, u_m) . Below we both define W and present our analysis in terms of Euclidean spaces. It therefore follows that our findings, in principle, are directly applicable to discrete versions of (3)-(4). On the other hand, practical use would require that a number of involved technical issues are handled: one must construct suitable geometrical models, obtain EEC or ECG recordings, handle noisy data, etc.

Solving inverse source problems using optimization procedures is challenging. For example, the minimizer $f_\alpha \in F_h \subset L^2(\Omega)$ of

$$\min_{(f,u) \in F_h \times H^1(\Omega)} \left\{ \frac{1}{2} \|u - d\|_{L^2(\partial\Omega)}^2 + \frac{1}{2} \alpha \|f\|_{L^2(\Omega)}^2 \right\}$$

subject to

$$\begin{aligned} -\Delta u + \epsilon u &= f \quad \text{in } \Omega, \\ \frac{\partial u}{\partial \mathbf{n}} &= 0 \quad \text{on } \partial\Omega, \end{aligned}$$

is not, in general, a good approximation of a true interior source: Even if the data d is generated from a single basis function $\phi_j \in F_h$, representing an interior local source, the minimum L^2 -norm least-squares solution $f^* = \lim_{\alpha \rightarrow 0} f_\alpha$ will attain its maximum at the boundary $\partial\Omega$ of the domain Ω , see [10]. However,

by employing a carefully chosen regularization operator W and an orthonormal basis for F_h , we proved in [10] that $W^{-1}f^*$ attains its maximum at the position of the true local source ϕ_j . On the other hand, $W^{-1}f^*$ is very smooth and its magnitude will typically not be close to the magnitude of the true source.

The need for sparse solutions in many applications, as exemplified above, thus motivates the study of ℓ^1 -regularization for inverse source problems. We now present a brief overview of the main results of our forthcoming analysis.

Assume that the Dirichlet boundary data $d \in L^2(\partial\Omega)$ in (1) is generated from a basis function $\phi_j \in F_h$, i.e., $d = K_h\phi_j$, where

$$K_h : F_h \rightarrow L^2(\partial\Omega), \quad f \mapsto u|_{\partial\Omega},$$

is the forward operator associated with (1)-(2). Provided that W denotes the above-mentioned regularization operator introduced in [10], we will prove that ϕ_j is the unique solution of

$$\min_{f \in F_h} \|Wf\|_1 \quad \text{subject to} \quad K_h f = K_h \phi_j.$$

We will further show, using a slightly modified fidelity term in (1)-(2), that the associated minimizer of the weighted ℓ^1 -regularized problem is

$$f_\alpha = \gamma_\alpha \phi_j,$$

where $\gamma_\alpha = 1 - c\alpha$, and c is a positive constant. That is, the correct basis function is recovered without any blurring for all values of $\alpha < \bar{\alpha}$, albeit with an error in magnitude equal to $c\alpha$. The constants $\bar{\alpha}$ and c can be computed from W and a projection operator.

3 Analysis

For the sake of clarity, we will present our theoretical results in terms of Euclidean spaces, employing the standard inner product and the standard basis vectors. It should be noted that analogous results can be established for linear operators acting on finite dimensional vector spaces, provided that an orthonormal basis is employed for the domain of the operators.

Consider the problem

$$\min_{\mathbf{x} \in \mathbb{R}^n} \left\{ \frac{1}{2} \|\mathbf{A}\mathbf{x} - \mathbf{b}\|_2^2 + \alpha \|\mathbf{W}\mathbf{x}\|_1 \right\}, \quad (5)$$

where $\mathbf{A} \in \mathbb{R}^{m \times n}$ has a non-trivial nullspace² $\mathcal{N}(\mathbf{A})$. Associated with \mathbf{A} is the orthogonal projection matrix

$$\mathbf{P} : \mathbb{R}^n \rightarrow \mathcal{N}(\mathbf{A})^\perp. \quad (6)$$

²Our analysis also holds for matrices with linearly independent columns, but this is the trivial case.

That is, $\mathbf{P} = \mathbf{A}^\dagger \mathbf{A}$, where \mathbf{A}^\dagger denotes the Moore-Penrose inverse of \mathbf{A} . For the inverse problems of EEG and ECG, \mathbf{A} would be the aforementioned transfer matrix.

Throughout this paper, the diagonal regularization matrix $\mathbf{W} \in \mathbb{R}^{n \times n}$ is defined as

$$\mathbf{W}\mathbf{e}_i = \|\mathbf{P}\mathbf{e}_i\|_2 \mathbf{e}_i, \quad i = 1, 2, \dots, n, \quad (7)$$

where we assume that $\mathbf{P}\mathbf{e}_i \neq 0$, $i = 1, 2, \dots, n$. The definition of this matrix can be motivated by the classical theory for the minimum norm least squares solution of linear systems and Tikhonov regularization, see [10] for further details. Furthermore, the beneficial mathematical properties of this operator in connection with quadratic regularization are studied in [10, 11]. Below it will become clear that (7) also plays an important role for developing sparsity promoting regularization techniques.

The main purpose of this section is to analyze whether we can recover a standard basis vector $\mathbf{e}_j \in \mathbb{R}^n$ from the exact data $\mathbf{b}^\dagger = \mathbf{A}\mathbf{e}_j$. Our starting point is thus the following optimization problem.

- **Problem 0:**

$$\min_{\mathbf{x} \in \mathbb{R}^n} \left\{ \frac{1}{2} \|\mathbf{A}\mathbf{x} - \mathbf{b}^\dagger\|_2^2 + \alpha \|\mathbf{W}\mathbf{x}\|_1 \right\}. \quad (8)$$

3.1 Weighted basis pursuit

Our first result concerns the solution of Problem 0 in the limit $\alpha \rightarrow 0$. Recalling that $\mathbf{b}^\dagger = \mathbf{A}\mathbf{e}_j$, it is well-known that this limit problem can be formulated as

- **Problem I:**

$$\min_{\mathbf{x} \in \mathbb{R}^n} \|\mathbf{W}\mathbf{x}\|_1 \quad \text{subject to} \quad \mathbf{A}\mathbf{x} = \mathbf{A}\mathbf{e}_j.$$

We also introduce an equivalent formulation of Problem I, which reads

- **Problem II:**

$$\min_{\mathbf{x} \in \mathbb{R}^n} \|\mathbf{W}\mathbf{x}\|_1 \quad \text{subject to} \quad \mathbf{P}\mathbf{x} = \mathbf{P}\mathbf{e}_j.$$

Problems I and II are equivalent because the nullspaces of \mathbf{A} and \mathbf{P} coincide, i.e., $\mathcal{N}(\mathbf{A}) = \mathcal{N}(\mathbf{P})$. Hence, either problem can be reformulated as

$$\min_{\mathbf{q} \in \mathcal{N}(\mathbf{A})} \|\mathbf{W}(\mathbf{e}_j + \mathbf{q})\|_1.$$

We will assume that no *two* columns of \mathbf{A} are parallel in order to ensure that the solution of our minimization problems is *unique*.

Assumption 3.1. *We assume that $\mathbf{A} \in \mathbb{R}^{m \times n}$ is such that $\mathbf{A}\mathbf{e}_j \neq c\mathbf{A}\mathbf{e}_i$ for all $i, j \in \{1, 2, \dots, n\}$, $i \neq j$, and all $c \in \mathbb{R}$.*

Note that this assumption implies that $\mathbf{e}_i \notin \mathcal{N}(A)$, $i \in \{1, 2, \dots, n\}$. Furthermore, invoking the orthogonal decomposition $\mathbf{e}_i = \mathbf{P}\mathbf{e}_i + (\mathbf{e}_i - \mathbf{P}\mathbf{e}_i)$, where $(\mathbf{e}_i - \mathbf{P}\mathbf{e}_i) \in \mathcal{N}(A)$, it follows that $\mathbf{A}\mathbf{e}_i = \mathbf{A}\mathbf{P}\mathbf{e}_i$. Consequently, if \mathbf{A} obeys Assumption 3.1, then \mathbf{P} must also satisfy

$$\mathbf{P}\mathbf{e}_j \neq c\mathbf{P}\mathbf{e}_i \text{ for all } i, j \in \{1, 2, \dots, n\}, i \neq j, \text{ and all } c \in \mathbb{R}. \quad (9)$$

We can now formulate our first result. Let us remark that the study of sparsity promoting regularization techniques usually leads to very involved mathematical analysis. However, with the very specific choice of the weight matrix \mathbf{W} in (7) and the data $\mathbf{b}^\dagger = \mathbf{A}\mathbf{e}_j$, our analysis becomes rather "transparent".

Theorem 3.2 (Exact recovery of a basis vector). *Assume that $\mathbf{A} \in \mathbb{R}^{m \times n}$ satisfies Assumption 3.1, and let \mathbf{P} and \mathbf{W} be the matrices defined in (6) and (7), respectively. Then \mathbf{e}_j is the unique solution of problems I and II.*

Proof. Problem I and Problem II are equivalent. We choose to consider the latter, i.e.,

$$\min_{\mathbf{x} \in \mathbb{R}^n} \|\mathbf{W}\mathbf{x}\|_1 \quad \text{subject to} \quad \mathbf{P}\mathbf{x} = \mathbf{P}\mathbf{e}_j.$$

Define $X_j = \{\mathbf{x} \in \mathbb{R}^n : \mathbf{P}\mathbf{x} = \mathbf{P}\mathbf{e}_j\}$. Let $\mathbf{x} = \sum_i c_i \mathbf{e}_i \in X_j, \mathbf{x} \neq \mathbf{e}_j$ be arbitrary. Then, see (7),

$$\begin{aligned} \|\mathbf{W}\mathbf{e}_j\|_1 &= \|\|\mathbf{P}\mathbf{e}_j\|_2 \mathbf{e}_j\|_1 \\ &= \|\mathbf{P}\mathbf{e}_j\|_2 \\ &= \left\| \mathbf{P} \left(\sum_i c_i \mathbf{e}_i \right) \right\|_2 \\ &= \left\| \sum_i c_i \mathbf{P}\mathbf{e}_i \right\|_2 \\ &\leq \sum_i |c_i| \|\mathbf{P}\mathbf{e}_i\|_2 \\ &= \left\| \sum_i c_i \|\mathbf{P}\mathbf{e}_i\|_2 \mathbf{e}_i \right\|_1 \\ &= \|\mathbf{W}\mathbf{x}\|_1. \end{aligned}$$

Using (9), which is a consequence of Assumption 3.1, we get strict inequality in the third to last step, and the result follows. \square

Theorem 3.2 states that a single basis vector \mathbf{e}_j can be exactly recovered from the data $\mathbf{b}^\dagger = \mathbf{A}\mathbf{e}_j$ by solving either Problem I or Problem II. If Assumption 3.1 does not hold, \mathbf{e}_j would still be a minimizer, but the uniqueness is not assured. (Similar statements hold for the remaining results presented in this paper.)

3.2 Alternative optimization problems

Inspired by Problem II, we now suggest an alternative to (5). Since $\mathbf{P} = \mathbf{A}^\dagger \mathbf{A}$, it follows that

$$\mathbf{P} \mathbf{e}_j = \mathbf{A}^\dagger \mathbf{A} \mathbf{e}_j = \mathbf{A}^\dagger \mathbf{b}^\dagger,$$

where $\mathbf{b}^\dagger = \mathbf{A} \mathbf{e}_j$. Consequently, for a general right-hand-side \mathbf{b} , Problem II motivates the following alternative to (5)

$$\min_{\mathbf{x} \in \mathbb{R}^n} \left\{ \frac{1}{2} \|\mathbf{P} \mathbf{x} - \mathbf{A}^\dagger \mathbf{b}\|_2^2 + \alpha \|\mathbf{W} \mathbf{x}\|_1 \right\}. \quad (10)$$

As far as we understand, it is difficult to motivate (10) by a practical challenge. On the other hand, in view of Problem II and the theory for the minimum norm least squares solution one might expect that investigating (10) is relevant.

If \mathbf{A} has very small singular values, it may not be advisable to apply \mathbf{A}^\dagger in practise. Therefore we want to approximate \mathbf{A}^\dagger with a more well-behaved matrix. This can, e.g., be accomplished by employing the truncated SVD to get an approximation \mathbf{A}_k of \mathbf{A} . Here, $k \leq m$ represents the number of singular values that are unchanged in the truncation: Assuming that the singular values of \mathbf{A} are sorted in decreasing order $\sigma_1 \geq \sigma_2 \geq \dots \geq \sigma_m$, \mathbf{A}_k will have the singular values $\sigma_1 \geq \sigma_2 \geq \dots \geq \sigma_k \geq 0 = 0 = \dots = 0$.

Below we need the orthogonal projection onto the orthogonal complement of the nullspace of \mathbf{A}_k ,

$$\mathbf{P}_k : \mathbb{R}^n \rightarrow \mathcal{N}(\mathbf{A}_k)^\perp. \quad (11)$$

And, analogously to (7), we define

$$\mathbf{W}_k \mathbf{e}_i = \|\mathbf{P}_k \mathbf{e}_i\|_2 \mathbf{e}_i, \quad i = 1, 2, \dots, n. \quad (12)$$

Replacing \mathbf{A}^\dagger in (10) with \mathbf{A}_k^\dagger , keeping in mind that $\mathbf{P} = \mathbf{A}^\dagger \mathbf{A}$, leads to the following alternative to (5)

$$\min_{\mathbf{x} \in \mathbb{R}^n} \left\{ \frac{1}{2} \|\mathbf{A}_k^\dagger \mathbf{A} \mathbf{x} - \mathbf{A}_k^\dagger \mathbf{b}\|_2^2 + \alpha \|\mathbf{W}_k \mathbf{x}\|_1 \right\}. \quad (13)$$

Note that we have also replaced \mathbf{W} with \mathbf{W}_k .

From the SVD of $\mathbf{A} = \mathbf{U} \mathbf{\Sigma} \mathbf{V}^T$, we find the SVD of \mathbf{A}_k ,

$$\mathbf{A}_k = \mathbf{U} \mathbf{\Sigma}_k \mathbf{V}^T.$$

Observe that

$$\mathbf{P}_k = \mathbf{A}_k^\dagger \mathbf{A}_k = \mathbf{V} \mathbf{\Sigma}_k^\dagger \mathbf{\Sigma}_k \mathbf{V}^T,$$

and that

$$\mathbf{A}_k^\dagger \mathbf{A} = \mathbf{V} \mathbf{\Sigma}_k^\dagger \mathbf{\Sigma} \mathbf{V}^T.$$

This yields, since $\mathbf{\Sigma}_k^\dagger \mathbf{\Sigma}_k = \mathbf{\Sigma}_k^\dagger \mathbf{\Sigma}$,

$$\mathbf{P}_k = \mathbf{A}_k^\dagger \mathbf{A}, \quad (14)$$

and we can write (13) in the form

$$\min_{\mathbf{x} \in \mathbb{R}^n} \left\{ \frac{1}{2} \|\mathbf{P}_k \mathbf{x} - \mathbf{A}_k^\dagger \mathbf{b}\|_2^2 + \alpha \|\mathbf{W}_k \mathbf{x}\|_1 \right\}. \quad (15)$$

In the next subsections we will analyze (10) and (15) when $\mathbf{b} = \mathbf{A}\mathbf{e}_j$ and $\mathbf{b} = \mathbf{A}\mathbf{e}_j + \eta$, respectively, where η represents noise.

3.3 Analysis of regularized problems

In this subsection we will make use of the following maximum property derived in [10]:

$$j \in \arg \max_{i \in \{1, 2, \dots, n\}} [\mathbf{W}^{-1} \mathbf{P} \mathbf{e}_j]_i,$$

where $[\mathbf{W}^{-1} \mathbf{P} \mathbf{e}_j]_i$ denotes the i 'th component of the vector $\mathbf{W}^{-1} \mathbf{P} \mathbf{e}_j$, and \mathbf{P} and \mathbf{W} are defined in (6) and (7), respectively. The proof of this is short, so we include it for the sake of completeness:

$$\begin{aligned} \mathbf{W}^{-1} \mathbf{P} \mathbf{e}_j &= \mathbf{W}^{-1} \sum_{i=1}^n (\mathbf{P} \mathbf{e}_j, \mathbf{e}_i) \mathbf{e}_i \\ &= \sum_{i=1}^n (\mathbf{P} \mathbf{e}_j, \mathbf{e}_i) \|\mathbf{P} \mathbf{e}_i\|^{-1} \mathbf{e}_i \\ &= \sum_{i=1}^n (\mathbf{P} \mathbf{e}_j, \mathbf{P} \mathbf{e}_i) \|\mathbf{P} \mathbf{e}_i\|^{-1} \mathbf{e}_i \\ &= \|\mathbf{P} \mathbf{e}_j\| \sum_{i=1}^n \left(\frac{\mathbf{P} \mathbf{e}_j}{\|\mathbf{P} \mathbf{e}_j\|}, \frac{\mathbf{P} \mathbf{e}_i}{\|\mathbf{P} \mathbf{e}_i\|} \right) \mathbf{e}_i. \end{aligned}$$

Furthermore, it is shown in [11] that, whenever Assumption 3.1 holds, we have the stronger property

$$j = \arg \max_{i \in \{1, 2, \dots, n\}} |[\mathbf{W}^{-1} \mathbf{P} \mathbf{e}_j]_i|. \quad (16)$$

With $\mathbf{b} = \mathbf{A}\mathbf{e}_j$, (10) reads

• **Problem III:**

$$\min_{\mathbf{x} \in \mathbb{R}^n} \left\{ \frac{1}{2} \|\mathbf{P} \mathbf{x} - \mathbf{P} \mathbf{e}_j\|_2^2 + \alpha \|\mathbf{W} \mathbf{x}\|_1 \right\}. \quad (17)$$

We will now see that the maximum property (16) yields an analysis of this problem which only involves classical convex optimization theory.

Theorem 3.3. *Assume that the matrix $\mathbf{A} \in \mathbb{R}^{m \times n}$ satisfies Assumption 3.1, and let \mathbf{P} and \mathbf{W} be the matrices defined in (6) and (7), respectively. Then*

$$\mathbf{x}_\alpha^* = \gamma_{j, \alpha} \mathbf{e}_j$$

is the unique solution of Problem III, where

$$\gamma_{j,\alpha} = 1 - \frac{\alpha}{[\mathbf{W}^{-1}\mathbf{P}\mathbf{e}_j]_j} \quad \text{for } 0 < \alpha < [\mathbf{W}^{-1}\mathbf{P}\mathbf{e}_j]_j. \quad (18)$$

Proof.

Existence: Let us define the cost-functional $\mathcal{J} : \mathbb{R}^n \rightarrow \mathbb{R}$ associated with (17),

$$\mathcal{J}(\mathbf{x}) = \underbrace{\frac{1}{2}\|\mathbf{P}\mathbf{x} - \mathbf{P}\mathbf{e}_j\|_2^2}_{=g(\mathbf{x})} + \underbrace{\alpha\|\mathbf{W}\mathbf{x}\|_1}_{=\alpha h(\mathbf{W}\mathbf{x})}, \quad (19)$$

where $g(\cdot)$ and $h(\mathbf{W}\cdot)$ represent the fidelity and regularization terms, respectively. According to standard convex optimization theory, \mathbf{x} is a minimizer of \mathcal{J} if and only if

$$\begin{aligned} \mathbf{0} &\in \partial\mathcal{J}(\mathbf{x}) \\ &= \nabla g(\mathbf{x}) + \alpha\mathbf{W}^T\partial h(\mathbf{W}\mathbf{x}). \end{aligned}$$

where " ∂ " denotes the subgradient. Since $\mathbf{W}^T = \mathbf{W}$, we can multiply with \mathbf{W}^{-1} to obtain

$$-\mathbf{W}^{-1}\nabla g(\mathbf{x}) \in \alpha\partial h(\mathbf{W}\mathbf{x}),$$

and from the expression for g we find, keeping in mind that $\mathbf{P}^T\mathbf{P} = \mathbf{P}\mathbf{P} = \mathbf{P}$,

$$\mathbf{W}^{-1}\mathbf{P}(\mathbf{e}_j - \mathbf{x}) \in \alpha\partial h(\mathbf{W}\mathbf{x}). \quad (20)$$

We also observe, using the fact that $h(\mathbf{y}) = \|\mathbf{y}\|_1$ and that \mathbf{W} is a diagonal matrix with positive entries at its diagonal,

$$[\partial h(\mathbf{W}\mathbf{x})]_i = [\partial h(\mathbf{W}[x_1 \ x_2 \ \dots \ x_n]^T)]_i = \begin{cases} \{1\}, & x_i > 0, \\ \{-1\}, & x_i < 0, \\ [-1, 1], & x_i = 0. \end{cases}$$

We will now investigate whether there exists a scalar γ such that $\mathbf{x} = \gamma\mathbf{e}_j$ satisfies the optimality criterion (20). Note that, for $\gamma > 0$,

$$[\partial h(\mathbf{W}\gamma\mathbf{e}_j)]_i = \begin{cases} \{1\}, & i = j, \\ [-1, 1], & i \neq j, \end{cases} \quad (21)$$

and the condition (20) becomes

$$(1 - \gamma)[\mathbf{W}^{-1}\mathbf{P}\mathbf{e}_j]_i \in \alpha \begin{cases} \{1\}, & i = j, \\ [-1, 1], & i \neq j. \end{cases} \quad (22)$$

Setting

$$\gamma = \gamma_{j,\alpha} = 1 - \frac{\alpha}{[\mathbf{W}^{-1}\mathbf{P}\mathbf{e}_j]_j}, \quad (23)$$

we observe from (16) that

$$(1 - \gamma_{j,\alpha})[W^{-1}P\mathbf{e}_j]_i = \alpha \frac{[W^{-1}P\mathbf{e}_j]_i}{[W^{-1}P\mathbf{e}_j]_j} \in \alpha \begin{cases} \{1\}, & i = j, \\ (-1, 1), & i \neq j, \end{cases} \quad (24)$$

and we conclude that (22) holds for the particular choice (23) of γ .

This argument shows that $\mathbf{x}_\alpha^* = \gamma_{j,\alpha}\mathbf{e}_j$ is a minimizer of \mathcal{J} . The next step is to use the property that $(1 - \gamma_{j,\alpha})[W^{-1}P\mathbf{e}_j]_i$ is contained in the open interval $(-\alpha, \alpha)$, $i \neq j$, to prove the uniqueness.

Uniqueness: We have determined a minimizer $\mathbf{x}_\alpha^* = \gamma_{j,\alpha}\mathbf{e}_j$ of \mathcal{J} . Let $\mathbf{y} \in \mathbb{R}^n, \mathbf{y} \neq \mathbf{x}_\alpha^*$, be arbitrary. We will show that

$$\mathcal{J}(\mathbf{y}) > \mathcal{J}(\mathbf{x}_\alpha^*).$$

If $\mathbf{y} = c\mathbf{x}_\alpha^*$, $c \neq 1$, it follows from the analysis presented above that this is not a minimizer of \mathcal{J} . Consequently, for the remaining part of the proof we assume that $\mathbf{y} \neq c\mathbf{x}_\alpha^*$. In particular, this implies that at least one of the components, say y_k , $k \neq j$, of \mathbf{y} is such that $y_k \neq 0$.

Recall the definition (19) of \mathcal{J} , g and h and that, using the definition of the subgradient,

$$h(W\mathbf{y}) - h(W\mathbf{x}_\alpha^*) \geq \mathbf{z}^T(W\mathbf{y} - W\mathbf{x}_\alpha^*) \quad \text{for all } \mathbf{z} \in \partial h(W\mathbf{x}_\alpha^*).$$

Therefore

$$\begin{aligned} \mathcal{J}(\mathbf{y}) - \mathcal{J}(\mathbf{x}_\alpha^*) &= g(\mathbf{y}) + \alpha h(W\mathbf{y}) - g(\mathbf{x}_\alpha^*) - \alpha h(W\mathbf{x}_\alpha^*) \\ &\geq \frac{1}{2}\|P\mathbf{y} - P\mathbf{e}_j\|_2^2 - \frac{1}{2}\|P\mathbf{x}_\alpha^* - P\mathbf{e}_j\|_2^2 \\ &\quad + \alpha \mathbf{z}^T W(\mathbf{y} - \mathbf{x}_\alpha^*) \quad \text{for all } \mathbf{z} \in \partial h(W\mathbf{x}_\alpha^*). \end{aligned} \quad (25)$$

Since $\mathbf{x}_\alpha^* = \gamma_{j,\alpha}\mathbf{e}_j$, we can write (24) as

$$\begin{aligned} [W^{-1}P(\mathbf{e}_j - \mathbf{x}_\alpha^*)]_i &\in \alpha \begin{cases} \{1\}, & i = j \\ (-1, 1), & i \neq j \end{cases} \\ &\subset \alpha \begin{cases} \{1\}, & i = j \\ [-1, 1], & i \neq j \end{cases} \\ &= \alpha[\partial h(W\mathbf{x}_\alpha^*)]_i, \end{aligned} \quad (26)$$

see (21), i.e.,

$$\frac{1}{\alpha}W^{-1}P(\mathbf{e}_j - \mathbf{x}_\alpha^*) \in \partial h(W\mathbf{x}_\alpha^*). \quad (27)$$

Hence, we could choose $\mathbf{z} = \frac{1}{\alpha}W^{-1}P(\mathbf{e}_j - \mathbf{x}_\alpha^*)$ in (25), but then we do not (directly) get a strict inequality. Recall that \mathbf{y} has a component $y_k \neq 0$, where

$k \neq j$. Without loss of generality, we may assume that $[\mathbf{W}\mathbf{y} - \mathbf{W}\mathbf{x}_\alpha^*]_k > 0$. Define $\tilde{\mathbf{z}} = [\tilde{z}_1 \ \tilde{z}_2 \ \dots \ \tilde{z}_n]^T$ as follows³

$$\tilde{z}_i = \begin{cases} 1, & i = k, \\ \frac{1}{\alpha}[\mathbf{W}^{-1}\mathbf{P}(\mathbf{e}_j - \mathbf{x}_\alpha^*)]_i, & i \neq k. \end{cases}$$

Since (26) implies that $|\frac{1}{\alpha}[\mathbf{W}^{-1}\mathbf{P}(\mathbf{e}_j - \mathbf{x}_\alpha^*)]_k| < 1$, we find that

$$\tilde{\mathbf{z}}^T[\mathbf{W}\mathbf{y} - \mathbf{W}\mathbf{x}_\alpha^*] > \frac{1}{\alpha}[\mathbf{W}^{-1}\mathbf{P}(\mathbf{e}_j - \mathbf{x}_\alpha^*)]^T[\mathbf{W}\mathbf{y} - \mathbf{W}\mathbf{x}_\alpha^*].$$

Due to (26) and (21), $\tilde{\mathbf{z}} \in \partial h(\mathbf{W}\mathbf{x}_\alpha^*)$, and therefore (25) yields

$$\begin{aligned} \mathcal{J}(\mathbf{y}) - \mathcal{J}(\mathbf{x}_\alpha^*) &\geq \frac{1}{2}\|\mathbf{P}\mathbf{y} - \mathbf{P}\mathbf{e}_j\|_2^2 - \frac{1}{2}\|\mathbf{P}\mathbf{x}_\alpha^* - \mathbf{P}\mathbf{e}_j\|_2^2 \\ &\quad + \alpha\tilde{\mathbf{z}}^T\mathbf{W}(\mathbf{y} - \mathbf{x}_\alpha^*) \\ &> \frac{1}{2}\|\mathbf{P}\mathbf{y} - \mathbf{P}\mathbf{e}_j\|_2^2 - \frac{1}{2}\|\mathbf{P}\mathbf{x}_\alpha^* - \mathbf{P}\mathbf{e}_j\|_2^2 \\ &\quad + \alpha\frac{1}{\alpha}[\mathbf{W}^{-1}\mathbf{P}(\mathbf{e}_j - \mathbf{x}_\alpha^*)]^T[\mathbf{W}\mathbf{y} - \mathbf{W}\mathbf{x}_\alpha^*] \\ &= \frac{1}{2}\|\mathbf{P}\mathbf{y} - \mathbf{P}\mathbf{e}_j\|_2^2 - \frac{1}{2}\|\mathbf{P}\mathbf{x}_\alpha^* - \mathbf{P}\mathbf{e}_j\|_2^2 \\ &\quad + [\mathbf{P}(\mathbf{e}_j - \mathbf{x}_\alpha^*)]^T[\mathbf{y} - \mathbf{x}_\alpha^*]. \end{aligned}$$

The gradient of g , see (19), is $\nabla g(x) = \mathbf{P}(\mathbf{x} - \mathbf{e}_j)$. Consequently, the convexity of g implies that

$$\begin{aligned} \mathcal{J}(\mathbf{y}) - \mathcal{J}(\mathbf{x}_\alpha^*) &> \frac{1}{2}\|\mathbf{P}\mathbf{y} - \mathbf{P}\mathbf{e}_j\|_2^2 - \frac{1}{2}\|\mathbf{P}\mathbf{x}_\alpha^* - \mathbf{P}\mathbf{e}_j\|_2^2 \\ &\quad - \nabla g(\mathbf{x}_\alpha^*)^T[\mathbf{y} - \mathbf{x}_\alpha^*] \\ &\geq \frac{1}{2}\|\mathbf{P}\mathbf{y} - \mathbf{P}\mathbf{e}_j\|_2^2 - \frac{1}{2}\|\mathbf{P}\mathbf{x}_\alpha^* - \mathbf{P}\mathbf{e}_j\|_2^2 \\ &\quad - [g(\mathbf{y}) - g(\mathbf{x}_\alpha^*)] \\ &= \frac{1}{2}\|\mathbf{P}\mathbf{y} - \mathbf{P}\mathbf{e}_j\|_2^2 - \frac{1}{2}\|\mathbf{P}\mathbf{x}_\alpha^* - \mathbf{P}\mathbf{e}_j\|_2^2 \\ &\quad - \left[\frac{1}{2}\|\mathbf{P}\mathbf{y} - \mathbf{P}\mathbf{e}_j\|_2^2 - \frac{1}{2}\|\mathbf{P}\mathbf{x}_\alpha^* - \mathbf{P}\mathbf{e}_j\|_2^2 \right] \\ &= 0, \end{aligned}$$

which finishes the proof. \square

This theorem shows that $\mathbf{x}_\alpha^* = \gamma_{j,\alpha}\mathbf{e}_j$ is the unique minimizer of (17). The solution of (17) is thus obtained by only changing the magnitude of the true source \mathbf{e}_j , where the scaling factor $\gamma_{j,\alpha} \rightarrow 1$ as $\alpha \rightarrow 0$.

³If $[\mathbf{W}\mathbf{y} - \mathbf{W}\mathbf{x}_\alpha^*]_k < 0$, define $\tilde{z}_k = -1$, etc.

3.3.1 Noisy observation data

As mentioned in subsection 3.2, it may not be advisable to apply the pseudo-inverse \mathbf{A}^\dagger in practical computations. We therefore now want to study (13) in more detail. Setting $\mathbf{b} = \mathbf{A}\mathbf{e}_j + \eta$ in (15), where $\eta \in \mathbb{R}^m$ represents noise, leads to

$$\min_{\mathbf{x} \in \mathbb{R}^n} \left\{ \frac{1}{2} \|\mathbf{P}_k \mathbf{x} - (\mathbf{A}_k^\dagger \mathbf{A} \mathbf{e}_j + \mathbf{A}_k^\dagger \eta)\|_2^2 + \alpha \|\mathbf{W}_k \mathbf{x}\|_1 \right\}.$$

Since $\mathbf{A}_k^\dagger \mathbf{A} = \mathbf{P}_k$, see (14), this problem can also be written in the form

• **Problem IV:**

$$\min_{\mathbf{x} \in \mathbb{R}^n} \left\{ \frac{1}{2} \|\mathbf{P}_k \mathbf{x} - (\mathbf{P}_k \mathbf{e}_j + \mathbf{A}_k^\dagger \eta)\|_2^2 + \alpha \|\mathbf{W}_k \mathbf{x}\|_1 \right\}. \quad (28)$$

Theorem 3.4. Assume that $\mathbf{A}_k \in \mathbb{R}^{m \times n}$ satisfies Assumption 3.1, and let \mathbf{P}_k and \mathbf{W}_k be the matrices defined in (11) and (12), respectively. Then

$$\mathbf{x}_{\alpha, \eta}^* = \gamma_{j, \alpha, \eta} \mathbf{e}_j$$

is the unique solution of Problem IV, where

$$\gamma_{j, \alpha, \eta} = 1 - \frac{\alpha + [\mathbf{W}_k^{-1} \mathbf{A}_k^\dagger \eta]_j}{[\mathbf{W}_k^{-1} \mathbf{P}_k \mathbf{e}_j]_j}. \quad (29)$$

In order for this to hold, α must obey

$$\max_{i \neq j} \frac{1 + |\tau_{ij}|}{1 - |\tau_{ij}|} \max_i \left| [\mathbf{W}_k^{-1} \mathbf{A}_k^\dagger \eta]_i \right| < \alpha < [\mathbf{W}_k^{-1} \mathbf{P}_k \mathbf{e}_j]_j - [\mathbf{W}_k^{-1} \mathbf{A}_k^\dagger \eta]_j, \quad (30)$$

where

$$\tau_{ij} = \frac{[\mathbf{W}_k^{-1} \mathbf{P}_k \mathbf{e}_j]_i}{[\mathbf{W}_k^{-1} \mathbf{P}_k \mathbf{e}_j]_j} \in (-1, 1), \quad i \neq j.$$

Proof. Following the same reasoning as in the proof of Theorem (3.3), we derive that $\mathbf{x}_\alpha^* = \gamma \mathbf{e}_j$ is a unique minimizer of (28) if and only if

$$(1 - \gamma)[\mathbf{W}_k^{-1} \mathbf{P}_k \mathbf{e}_j]_i - [\mathbf{W}_k^{-1} \mathbf{A}_k^\dagger \eta]_i \in \alpha \begin{cases} \{1\}, & i = j \\ (-1, 1), & i \neq j, \end{cases} \quad (31)$$

where we have used the fact that $\mathbf{P}_k^T = \mathbf{P}_k = \mathbf{A}_k^\dagger \mathbf{A}_k$, and consequently

$$\mathbf{P}_k^T \mathbf{A}_k^\dagger = \mathbf{A}_k^\dagger \mathbf{A}_k \mathbf{A}_k^\dagger = \mathbf{A}_k^\dagger.$$

The criterion (31) holds for $i = j$ if

$$\gamma = \gamma_{j, \alpha, \eta} = 1 - \frac{\alpha + [\mathbf{W}_k^{-1} \mathbf{A}_k^\dagger \eta]_j}{[\mathbf{W}_k^{-1} \mathbf{P}_k \mathbf{e}_j]_j} > 0.$$

Consequently, α must satisfy the upper bound

$$\alpha < [\mathbf{W}_k^{-1} \mathbf{P}_k \mathbf{e}_j]_j - [\mathbf{W}_k^{-1} \mathbf{A}_k^\dagger \eta]_j.$$

Furthermore, setting $\gamma = \gamma_{j,\alpha,\eta}$ in (31), the condition (31) for $i \neq j$ reads

$$\left(\alpha + [\mathbf{W}_k^{-1} \mathbf{A}_k^\dagger \eta]_j \right) \frac{[\mathbf{W}_k^{-1} \mathbf{P}_k \mathbf{e}_j]_i}{[\mathbf{W}_k^{-1} \mathbf{P}_k \mathbf{e}_j]_j} \in \left(-\alpha + [\mathbf{W}_k^{-1} \mathbf{A}_k^\dagger \eta]_i, \alpha + [\mathbf{W}_k^{-1} \mathbf{A}_k^\dagger \eta]_i \right). \quad (32)$$

Recall that $\tau_{ij} := \frac{[\mathbf{W}_k^{-1} \mathbf{P}_k \mathbf{e}_j]_i}{[\mathbf{W}_k^{-1} \mathbf{P}_k \mathbf{e}_j]_j} \in (-1, 1)$ for $i \neq j$, see (16), and (32) can thus be expressed as the two inequalities

$$\begin{aligned} (1 + \tau_{ij}) \alpha &> [\mathbf{W}_k^{-1} \mathbf{A}_k^\dagger \eta]_i - \tau_{ij} [\mathbf{W}_k^{-1} \mathbf{A}_k^\dagger \eta]_j, \\ (1 - \tau_{ij}) \alpha &> \tau_{ij} [\mathbf{W}_k^{-1} \mathbf{A}_k^\dagger \eta]_j - [\mathbf{W}_k^{-1} \mathbf{A}_k^\dagger \eta]_i. \end{aligned} \quad (33)$$

It turns out that both of these inequalities are satisfied if

$$\max_{i \neq j} \frac{1 + |\tau_{ij}|}{1 - |\tau_{ij}|} \max_i \left| [\mathbf{W}_k^{-1} \mathbf{A}_k^\dagger \eta]_i \right| < \alpha. \quad (34)$$

Let us end the proof by verifying that (33) holds if (34) is satisfied. Since $(1 + \tau_{ij}) > 0$, the requirement (33) can be written in the form

$$\alpha > \frac{[\mathbf{W}_k^{-1} \mathbf{A}_k^\dagger \eta]_i - \tau_{ij} [\mathbf{W}_k^{-1} \mathbf{A}_k^\dagger \eta]_j}{1 + \tau_{ij}}.$$

We derive the inequalities

$$\begin{aligned} \frac{[\mathbf{W}_k^{-1} \mathbf{A}_k^\dagger \eta]_i - \tau_{ij} [\mathbf{W}_k^{-1} \mathbf{A}_k^\dagger \eta]_j}{1 + \tau_{ij}} &\leq \frac{\left| [\mathbf{W}_k^{-1} \mathbf{A}_k^\dagger \eta]_i - \tau_{ij} [\mathbf{W}_k^{-1} \mathbf{A}_k^\dagger \eta]_j \right|}{|1 + \tau_{ij}|} \\ &\leq \frac{\left| [\mathbf{W}_k^{-1} \mathbf{A}_k^\dagger \eta]_i \right| + |\tau_{ij}| \left| [\mathbf{W}_k^{-1} \mathbf{A}_k^\dagger \eta]_j \right|}{1 - |\tau_{ij}|} \\ &\leq \max_{i \neq j} \frac{1 + |\tau_{ij}|}{1 - |\tau_{ij}|} \max_i \left| [\mathbf{W}_k^{-1} \mathbf{A}_k^\dagger \eta]_i \right|, \end{aligned}$$

and we conclude that: If α satisfies (34), then (33) holds. This finishes the proof. \square

Roughly, the left inequality in (30) ensures that the error amplification caused by the inverse solution procedure does not become too dominate, and the right inequality prevents the regularization term from becoming too “strong” and thereby yield a poor recovery of the source. This is the mathematical intuition for these inequalities. It is, however, difficult to provide a physical intuition for these constraints on α because these inequalities are linked to the smoothing properties of the forward operator associated with a concrete application.

Remark 3.5 (Several sources). Let us mention that the methods introduced in this paper can not, in general, guarantee the recovery of multiple sources. To show this, assume that the exact data is $\mathbf{b}^\dagger = \mathbf{A}\mathbf{e}_m + \mathbf{A}\mathbf{e}_n$ and that there exist a constant c and an index j such that $\mathbf{A}\mathbf{e}_m + \mathbf{A}\mathbf{e}_n = c\mathbf{A}\mathbf{e}_j$.

Recall that $\mathbf{P} = \mathbf{A}^\dagger \mathbf{A}$. Hence, multiplying $\mathbf{A}\mathbf{e}_m + \mathbf{A}\mathbf{e}_n = c\mathbf{A}\mathbf{e}_j$ with \mathbf{A}^\dagger yields

$$\mathbf{P}\mathbf{e}_m + \mathbf{P}\mathbf{e}_n = c\mathbf{P}\mathbf{e}_j.$$

The weighted basis pursuit problem, cf. Problem II, then reads

$$\min_{\mathbf{x} \in \mathbb{R}^n} \|\mathbf{W}\mathbf{x}\|_1 \quad \text{subject to} \quad \mathbf{P}\mathbf{x} = \mathbf{P}\mathbf{e}_m + \mathbf{P}\mathbf{e}_n.$$

Following the proof of Theorem 3.2, we get

$$\begin{aligned} \|c\mathbf{W}\mathbf{e}_j\|_1 &= |c| \|\mathbf{P}\mathbf{e}_j\|_2 \\ &= |c| \left\| \frac{\mathbf{P}\mathbf{e}_m + \mathbf{P}\mathbf{e}_n}{c} \right\|_2 \\ &= \|\mathbf{P}\mathbf{e}_m + \mathbf{P}\mathbf{e}_n\|_2 \\ &< \|\mathbf{P}\mathbf{e}_m\|_2 + \|\mathbf{P}\mathbf{e}_n\|_2 \\ &= \|\mathbf{W}(\mathbf{e}_m + \mathbf{e}_n)\|_1, \end{aligned}$$

where the strict inequality is a consequence of Assumption 3.1, see also (9). This argument shows that the two true sources \mathbf{e}_m and \mathbf{e}_n will not be recovered by solving Problem II. See Figure 2 for an illustration.

On the other hand, if there do not exist an index j and a constant c such that $\mathbf{A}\mathbf{e}_m + \mathbf{A}\mathbf{e}_n = c\mathbf{A}\mathbf{e}_j$, it is an open problem whether the weighted basis pursuit formulation can recover a 2-sparse vector. Or, more generally, can we recover a s -sparse solution if its image under \mathbf{A} is not equal to the image under \mathbf{A} of any s' -sparse solution with $s' < s$?

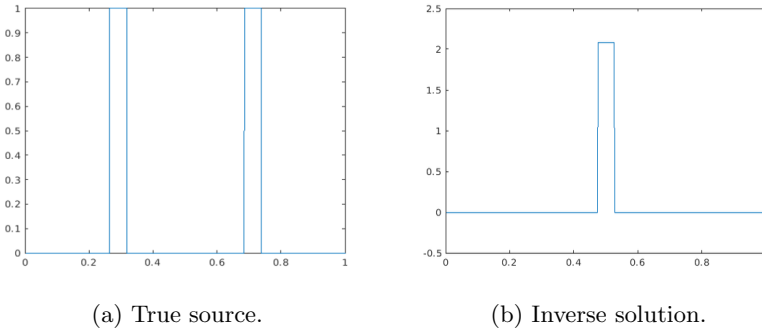


Figure 2: Panel (b) shows the solution f^* of (1)-(2) when $\Omega = (0, 1)$, $\epsilon = 1$ and $\alpha = 0.001$. The observation data d was in this case generated by the two true local sources depicted in Panel (a).

4 Numerical experiments

We committed the so-called "inverse crime" in Example 1: The same grid was used to both generate the boundary observation data d in (1) and for solving the inverse problem. In all the other experiments, the data d was generated using a finer grid for the state u than was used in the inverse computations. More specifically, $h_{\text{forward}} = 0.5h_{\text{inverse}}$, and we performed experiments on the unit square with 129×129 and 65×65 nodes for the forward and inverse computations of the state u , respectively. The control f was discretized in terms of a 16×16 mesh in all the simulations presented in examples 1-2 and 4. In Example 3, however, the true source was discretized using a finer 129×129 grid. Note that we employed the basis functions

$$\phi_i = \frac{1}{\|\mathcal{X}_{\Omega_i}\|_{L^2(\Omega)}} \mathcal{X}_{\Omega_i}, \quad i = 1, 2, \dots, n,$$

for F_h , where $\Omega_1, \Omega_2, \dots, \Omega_n$ are uniformly sized disjoint grid cells and \mathcal{X}_{Ω_i} denotes the characteristic function of Ω_i .

We employed the FEniCS software to generate the matrices involved in our experiments. Thereafter, the matrices were exported to MATLAB, where the optimization problems were solved with the split-Bregman algorithm [14]. We do not present a detailed description of the well-known mappings between the finite element spaces arising from the discretization of (1)-(2) to the Euclidean spaces used in (5), (10) and (15). Note, however, that $\mathbf{e}_j \in \mathbb{R}^n$ is associated with the FE basis function $\phi_j \in F_h \subset L^2(\Omega)$.

In all the simulations $\epsilon = 1$, see (2), and no noise was added to the data d , except in Example 2.

Figure 3 contains visualizations of the entries of the weight matrix W_k defined in (12). More specifically, each panel shows a plot of $\|\mathbf{P}_k \mathbf{e}_i\|$, $i = 1, 2, \dots, n$. We observe that the weights are largest for indexes associated with basis functions positioned close to the boundary of the domain Ω .

4.1 Example 1: Exact recovery of a single source

Figures 4 and 5 show numerical solutions of (10). In these problems we recover a single source and $\mathbf{b} = \mathbf{A}\mathbf{e}_j$. The theory developed for Problem III is therefore applicable, see Theorem 3.3. Figure 6 contains a comparison of the size of $\gamma_{j,\alpha}$, cf. (18), and the maximum value, $\max_i [\mathbf{x}_\alpha^*]_i$, of the solution \mathbf{x}_α^* of Problem III. We observe that the outcome of these experiments is as one could have anticipated from Theorem 3.3.

4.2 Example 2: Noise

If the observation data contains noise, it is natural to solve (15). Throughout this example, $k = 7$ in the truncated SVD employed to obtain the approximation \mathbf{A}_k of \mathbf{A} , see subsection 3.2. The experiment was executed as follows:

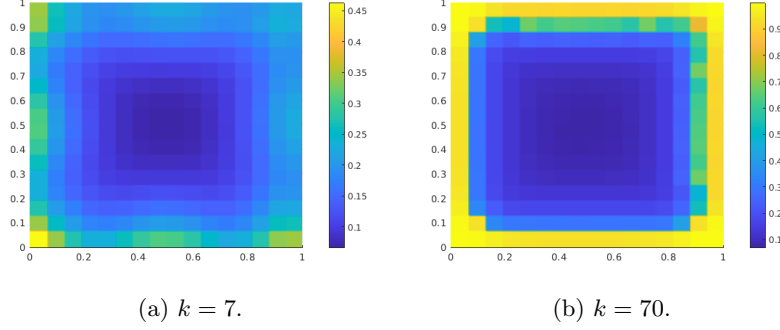


Figure 3: Visualizations of the matrix W_k . Panels (a) and (b) show plots of $\|P_k \mathbf{e}_i\|$, $i = 1, 2, \dots, n$, see (12), for two different choices of the truncation parameter k .

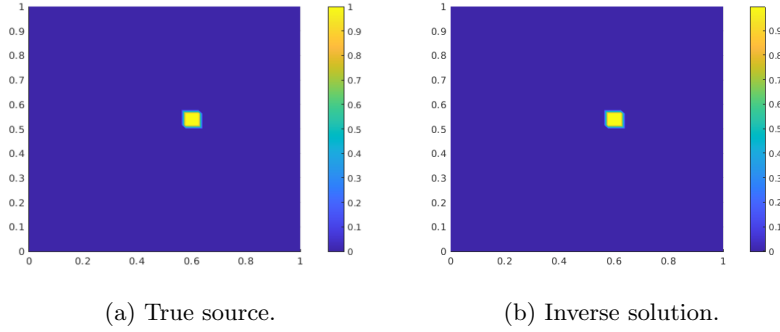


Figure 4: Comparison of a true *interior* source and the inverse solution computed by solving (10), Example 1. The size of the regularization parameter was $\alpha = 10^{-4}$.

1. Generate the data

$$\mathbf{b} = \mathbf{b}^\dagger + \eta = \mathbf{A}\mathbf{e}_j + \eta, \quad \eta = \delta\rho,$$

where δ is a scalar and ρ is a vector containing normally distributed numbers with zero mean and standard deviation equal to 1. See [10, Example 6] for a thorough discussion of the noise.

2. Compute $\mathbf{x}_k^* = \mathbf{A}_k^\dagger \mathbf{b} = \mathbf{A}_k^\dagger (\mathbf{A}\mathbf{e}_j + \eta)$, see (15).

3. Set

$$\bar{\alpha} = \max_{i \neq j} \frac{1 + |\tau_{ij}|}{1 - |\tau_{ij}|} \max_i \left| [\mathbf{W}_k^{-1} \mathbf{A}_k^\dagger \eta]_i \right|,$$

cf. Theorem 3.4.

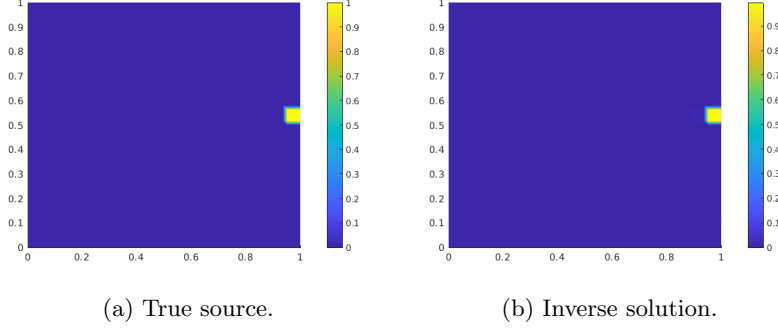


Figure 5: Comparison of a true source located at the *boundary* and the inverse solution computed by solving (10), Example 1. The size of the regularization parameter was $\alpha = 10^{-3}$.

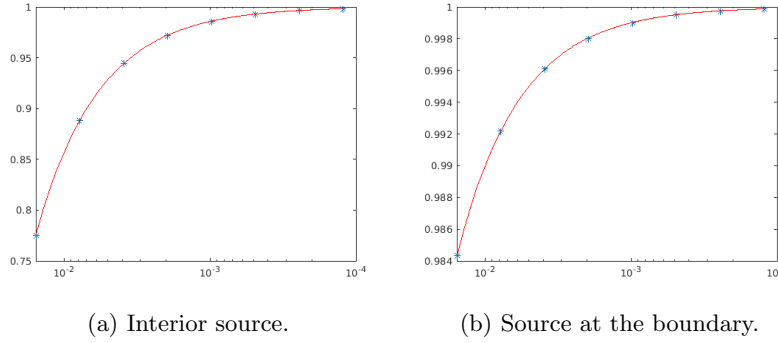


Figure 6: Example 1. The red curve shows the size of $\gamma_{j,\alpha}$, see (18), as a function of the regularization parameter α , and the asterisks represent $\max_i [\mathbf{x}_\alpha^*]_i$, where \mathbf{x}_α^* is the solution of (10).

4. Compute, see (15),

$$\mathbf{x}_\alpha^* = \arg \min_{\mathbf{x} \in \mathbb{R}^n} \left\{ \frac{1}{2} \|\mathbf{P}_k \mathbf{x} - \mathbf{x}_k^*\|_2^2 + \alpha \|\mathbf{W}_k \mathbf{x}\|_1 \right\}$$

for both $\alpha = 0.3\bar{\alpha}$ and $\alpha = 3\bar{\alpha}$.

This "setup" is such that the theory, presented in Theorem 3.4, for Problem IV is applicable.

Note that the problem is regularized in two steps. First with standard truncated SVD in Step 2 (i.e., the choice of the truncation parameter k), and then with ℓ^1 -regularization in Step 4 (i.e., the choice of α). How to optimally choose these parameters in relation to each other is a complicated matter and left for future research.

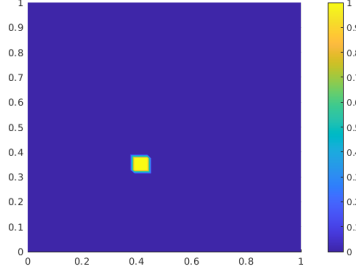


Figure 7: Example 2, true source.

Figure 8 compares over-regularized ($\alpha = 3\bar{\alpha}$) and under-regularized ($\alpha = 0.3\bar{\alpha}$) solutions of (15) with observation data containing 5% noise. Similar comparisons are presented in figures 9 and 10 for 10% and 15% noise, respectively. The true source is displayed in Figure 7.

When $\alpha = 3\bar{\alpha}$, the plots of \mathbf{x}_α^* , displayed in panels 8a), 9a) and 10a), show that the true source is successfully recovered in all three cases, albeit with an underestimated magnitude.

We can, however, as a post-processing step, improve the magnitude of the solutions using (29): Assuming $[\mathbf{W}_k^{-1}\mathbf{A}_k^\dagger\boldsymbol{\eta}]_j \ll [\mathbf{W}^{-1}\mathbf{P}_k\mathbf{e}_j]_j$, we compute

$$\mathbf{x}_{\alpha,\text{SCALED}}^* = \frac{\mathbf{x}_\alpha^*}{1 - \frac{\alpha}{[\mathbf{W}_k^{-1}\mathbf{P}_k\mathbf{e}_j]_j}},$$

where the index j in the denominator is known since $\arg \max_i \mathbf{x}_\alpha^* = j$. By rescaling the solution displayed in panel (a) of figures 8-10, the magnitude of the rescaled source becomes 0.88, 1.0 and 0.93, respectively. This post-processing step can only be mathematically justified if the assumptions needed in Theorem 3.4 hold, but it can "always" be applied in practice. (We have not explored its success when the assumptions in Theorem 3.4 are violated.)

When the problem is under-regularized, i.e., $\alpha = 0.3\bar{\alpha}$, the inverse solutions are still good visual approximations of the true source, see figures 8b), 9b) and 10b). However, the inverse solutions also contain small contributions from other basis vectors than \mathbf{e}_j . Both the magnitude and the number of incorrect active basis vectors appear to increase as the noise level increases.

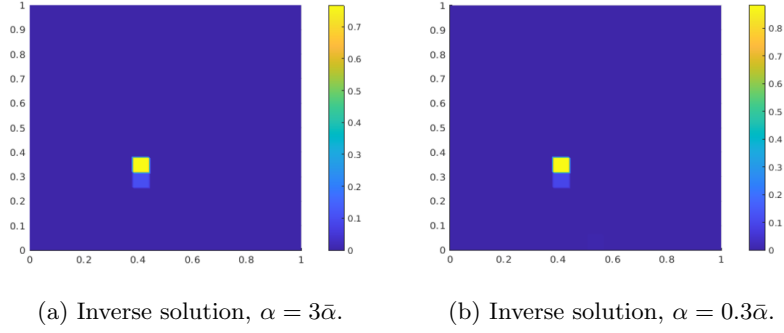


Figure 8: Example 2, 5% noise, $\bar{\alpha} = 0.0031$.

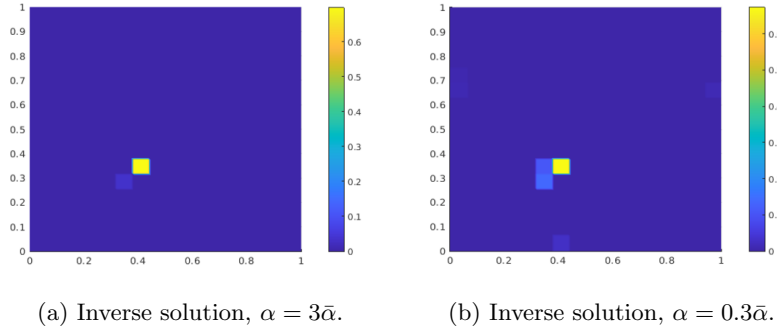


Figure 9: Example 2, 10% noise, $\bar{\alpha} = 0.0067$.

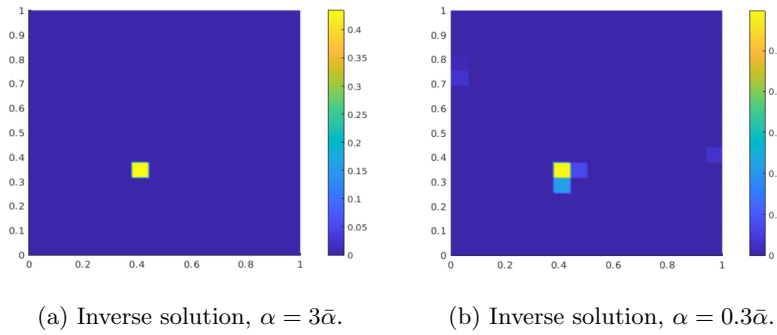


Figure 10: Example 2, 15% noise, $\bar{\alpha} = 0.0122$.

In most applications, $\bar{\alpha}$ is not available because it requires full knowledge of the noise. We therefore performed a numerical study under the common assumption that only (an estimate of) $\|\eta\|$ is known. This allows the use of

Morozov's discrepancy principle for choosing the truncation parameter k . Figure 11 compares solutions of (15) for different choices of k and α , where the choice $k = 5$ is obtained by applying Morozov's discrepancy principle with the threshold $1.05\|\eta\|$. The values $k = 3$ and $k = 15$ are chosen simply to compare the choice $k = 5$ with a smaller and larger truncation parameter.

In this particular example, we observe that using a relatively strong regularization in the truncated SVD step, i.e., choosing $k = 3$, gives good reconstruction of the source for all the tested values of α . If the regularization by truncated SVD is reduced, i.e., when k increases, it appears that α must be chosen more carefully to obtain a good reconstruction.

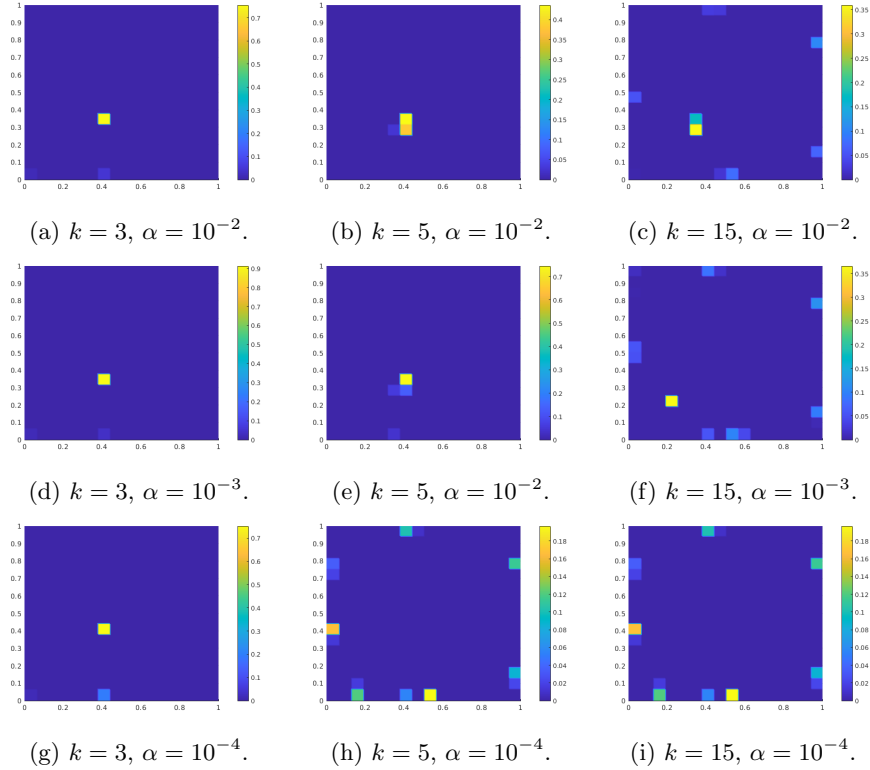


Figure 11: Example 2, 10% noise. Comparison of inverse solutions computed with different choices of the regularization parameters k and α . The choice $k = 5$ was the outcome of using Morozov's discrepancy principle with the threshold $1.05\|\eta\|$. Figure 7 shows the true source.

4.3 Example 3: Large circular source

So far we have considered examples covered by our analysis. We will now depart from this and explore more involved cases: The true source depicted in Figure

12(a) does not belong to the finite element space associated with the coarse mesh used to represent the control in the inverse computations.

We first note that Figure 12(b) shows that classical Tikhonov regularization

$$\min_{\mathbf{x} \in \mathbb{R}^n} \left\{ \frac{1}{2} \|\mathbf{A}\mathbf{x} - \mathbf{b}\|_2^2 + \gamma \|\mathbf{x}\|_2^2 \right\}, \quad (35)$$

with $\gamma = 10^{-4}$, fails to yield an adequate solution to this problem: Compare panels (a) and (b) of Figure 12. The mathematical explanation for this is presented in [10].

Next, we observe in Figure 13, left column, that the sparsity structure of the inverse solution computed by solving (15) deteriorates as the ℓ^1 -regularization parameter α tends to zero. However, for all three values of α , the position of the source is quite well recovered. In these simulations, the truncated SVD, employed to obtain the approximation \mathbf{A}_k^\dagger of the pseudo inverse \mathbf{A}^\dagger in (15), was obtained by choosing the truncation parameter $k = 5$.

As an alternative to the truncated SVD, we also used standard Tikhonov regularization to obtain an approximation of \mathbf{A}^\dagger , see subsection 3.2. More precisely, employing the singular value decomposition $\mathbf{A} = \mathbf{U}\Sigma\mathbf{V}^T$ of \mathbf{A} , the solution of the minimization problem

$$\min_{\hat{\mathbf{x}} \in \mathbb{R}^n} \left\{ \frac{1}{2} \|\mathbf{A}\hat{\mathbf{x}} - \mathbf{b}\|_2^2 + \frac{1}{2} \beta \|\hat{\mathbf{x}}\|_2^2 \right\},$$

can be expressed as

$$\hat{\mathbf{x}}_\beta = \mathbf{V}(\Sigma^2 + \beta\mathbf{I})^{-1} \mathbf{V}^T \mathbf{A}^T \mathbf{b} = \mathbf{S}_\beta \mathbf{b},$$

where

$$\mathbf{S}_\beta = \mathbf{V}(\Sigma^2 + \beta\mathbf{I})^{-1} \mathbf{V}^T \mathbf{A}^T \approx \mathbf{A}^\dagger. \quad (36)$$

Replacing \mathbf{A}^\dagger in (10) with \mathbf{S}_β , keeping in mind that $\mathbf{P} = \mathbf{A}^\dagger \mathbf{A}$, leads to the following alternative to (15)

$$\min_{\mathbf{x} \in \mathbb{R}^n} \left\{ \frac{1}{2} \|\mathbf{S}_\beta \mathbf{A} \mathbf{x} - \mathbf{S}_\beta \mathbf{b}\|_2^2 + \alpha \|\mathbf{W} \mathbf{x}\|_1 \right\}. \quad (37)$$

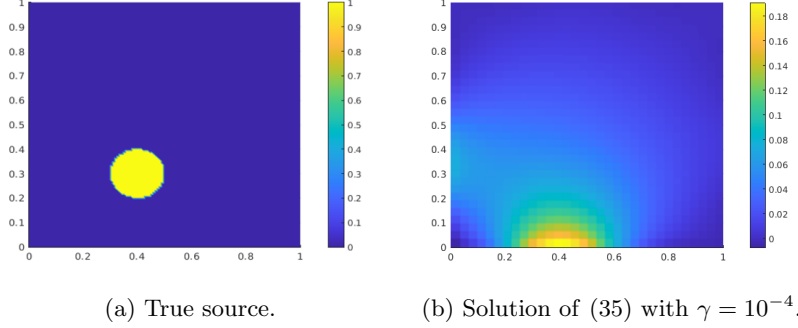


Figure 12: Example 3. Panel (a) shows the true source, and panel (b) displays the numerical solution of (1)-(2) using Tikhonov regularization $\gamma\|f\|_{L^2(\Omega)}^2$ instead of the weighted L^1 -regularization $\alpha\|Wf\|_{L^1(\Omega)}$.

The right column in Figure 13 contains the results obtained by solving (37). We observe, particularly for the two largest values of the ℓ^1 -regularization parameter α , that truncated SVD and Tikhonov regularization yield visually rather similar results.

4.4 Example 4: Multiple sources

Our last examples concern several sources. To solve the problems, we did the following:

1. For N true sources, we computed

$$\mathbf{b}^\dagger = A \left(\sum_{i=1}^N \mathbf{e}_{q_i} \right).$$

2. Thereafter, we solved the problem

$$\min_{\mathbf{x} \in \mathbb{R}^n} \left\{ \frac{1}{2} \|\mathbf{S}_\beta \mathbf{A} \mathbf{x} - \mathbf{S}_\beta \mathbf{b}^\dagger\|_2^2 + \alpha \|\mathbf{W} \mathbf{x}\|_1 \right\},$$

where \mathbf{S}_β is defined in (36).

Figure 14 contains results obtained with 2, 4 and 8 true sources. Panel b) shows that the two sources are nearly perfectly recovered. For the case with 4 sources, the inverse solution recovers three of the sources almost perfectly, while the fourth is 'split' into two adjacent sources with less magnitude, cf. Panel d). Panel f) shows the inverse solution for the case with 8 true sources, where we observe that the three sources located at the boundary are recovered very well (note the color bar), whereas the interior sources are merged somewhat into two clusters in the inverse solution.

5 Conclusions

If the exact data is generated from a single basis vector \mathbf{e}_j , our weighted ℓ^1 -regularization technique is able to exactly recover the true solution. When noise is present, we have obtained estimates for the size of the regularization parameter α which yield an inverse solution in the form $\gamma_{j,\alpha,\eta}\mathbf{e}_j$, where $\gamma_{j,\alpha,\eta}$ is a positive scalar. Numerical experiments suggest that our method also can, in many cases, identify several local sources, but we do not have a thorough mathematical understanding of this. We only know with certainty that it is possible to construct scenarios for which our scheme will fail to recover two sources.

Concerning the practical use of our weighted ℓ^1 -regularization method, it seems reasonable to expect that the method can recover two or three well-separated sources. Nevertheless, the definition of "well-separated" is problem dependent since it must depend on the smoothing properties of the involved forward operator and the geometry of the solution domain Ω . This means that one should, for each concrete application, perform a simulation study to explore which source patterns that can be identified by the weighted ℓ^1 -regularization method.

We defined our regularization operator and presented our analysis in terms of Euclidean spaces. Consequently, the methodology can be applied whenever a discrete version of a source identification task can be formulated in terms of a transfer matrix with a significant nullspace. For example, the use is not restricted to PDE-constrained optimization problems with elliptic state equations, but can also be applied when the state equation is parabolic or hyperbolic.

This study was motivated by inverse problems arising in connection with EEG and ECG recordings. In principle, our scheme can be applied to these problems, but a number of challenging engineering issues must be handled: one must construct suitable geometrical models (using, e.g., MR images), obtain EEG or ECG recordings, handle noisy data, etc. We intend to explore the EEG and ECG applications in forthcoming investigations.

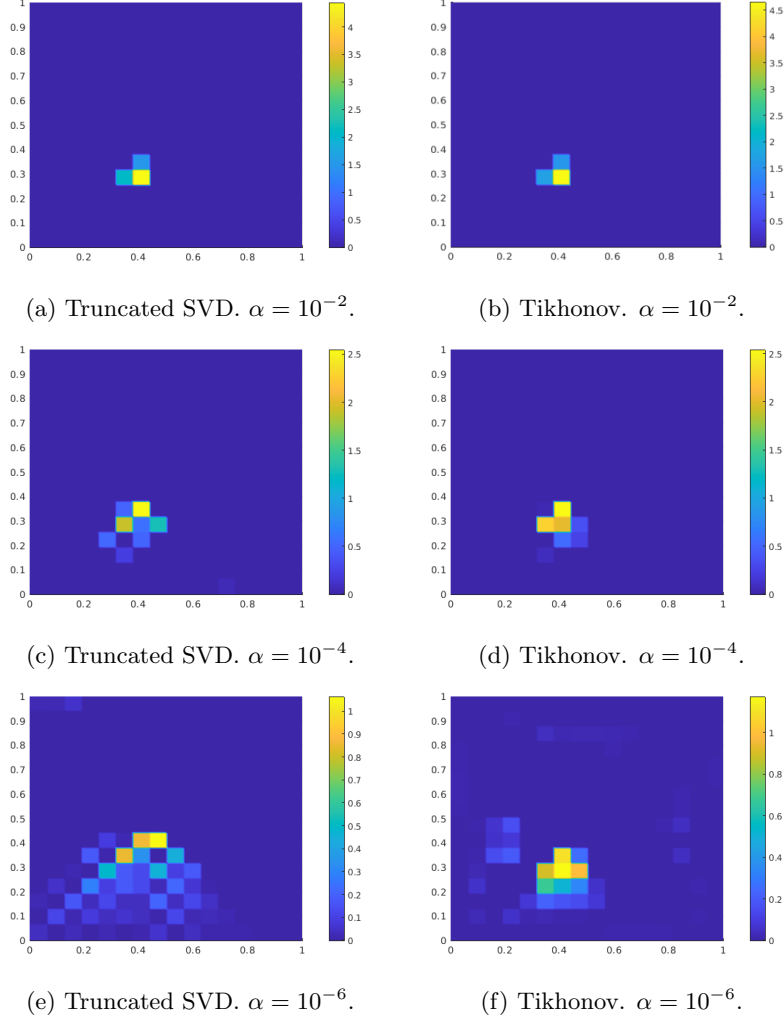


Figure 13: Example 3, employing weighted ℓ^1 -regularization $\alpha\|\mathbf{W}\mathbf{x}\|_1$. The inverse solutions were computed by solving (15) (approximating \mathbf{A}^\dagger with truncated SVD, $k = 5$) and (37) (approximating \mathbf{A}^\dagger with Tikhonov regularization, $\beta = 10^{-6}$). The true source is displayed in Figure 12(a).

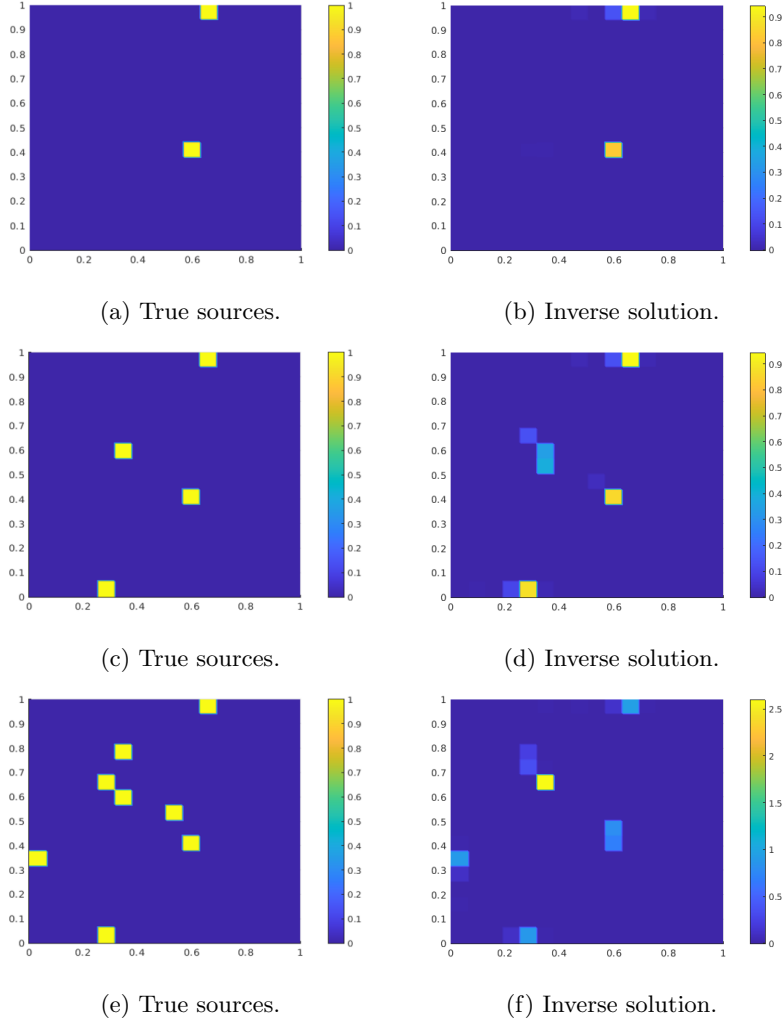


Figure 14: Example 4, recovering several local sources. Here, $\alpha = 0.01$ and $\beta = 10^{-6}$ in all the three experiments.

References

- [1] B. Abdelaziz, A. El Badia, and A. El Hajj. Direct algorithms for solving some inverse source problems in 2D elliptic equations. *Inverse Problems*, 31(10):105002, 2015.
- [2] A. Ben Abda, F. Ben Hassen, J. Leblond, and M. Mahjoub. Sources recovery from boundary data: A model related to electroencephalography. *Mathematical and Computer Modelling*, 49:2213–2223, 2009.

- [3] E. J. Candes, J. Romberg, and T. Tao. Robust uncertainty principles: exact signal reconstruction from highly incomplete frequency information. *IEEE Transactions on Information Theory*, 52(2):489–509, 2006.
- [4] E. J. Candes and T. Tao. Decoding by linear programming. *IEEE Transactions on Information Theory*, 51(12):4203–4215, 2005.
- [5] E. Casas, C. Clason, and K. Kunisch. Approximation of elliptic control problems in measure spaces with sparse solutions. *SIAM Journal on Control and Optimization*, 50(4):1735–1752, 2012.
- [6] X. Cheng, R. Gong, and W. Han. A new Kohn-Vogelius type formulation for inverse source problems. *Inverse Problems and Imaging*, 9(4):1051–1067, 2015.
- [7] I. Daubechies, M. Defrise, and C. De Mol. An iterative thresholding algorithm for linear inverse problems with a sparsity constraint. *Communications on Pure and Applied Mathematics*, 57(11):1413–1457, 2004.
- [8] D. L. Donoho and M. Elad. Optimally sparse representation in general (nonorthogonal) dictionaries via l_1 minimization. *Proceedings of the National Academy of Sciences*, 100(5):2197–2202, 2003.
- [9] A. El Badia and T. Ha-Duong. An inverse source problem in potential analysis. *Inverse Problems*, 16:651–663, 2000.
- [10] O. L. Elvetun and B. F. Nielsen. A regularization operator for source identification for elliptic PDEs. *To appear in Inverse Problems and Imaging*, arXiv:2005.09444, May 2020.
- [11] O. L. Elvetun and B. F. Nielsen. Modified Tikhonov regularization for identifying several sources. *arXiv e-prints*, page arXiv:2011.04394, 11 2020.
- [12] J. Flemming. Convergence rates for ℓ^1 -regularization without injectivity-type assumptions. *Inverse Problems*, 32(9), 2016.
- [13] S. Ghosh and Y. Rudy. Application of L_1 -norm regularization to epicardial potential solution of the inverse electrocardiography problem. *Annals of biomedical engineering*, 37(5):902–912, 2009.
- [14] T. Goldstein and S. Osher. The split Bregman method for l_1 -regularized problems. *SIAM Journal on Imaging Sciences*, 2:323–343, 2009.
- [15] A. Golmohammadi, M. R. M. Khaninezhad, and B. Jafarpour. *Exploiting Sparsity in Solving PDE-Constrained Inverse Problems: Application to Subsurface Flow Model Calibration*, pages 399–434. Springer New York, 2018.
- [16] M. Grasmair, M. Haltmeier, and O. Scherzer. Sparse regularization with l^q penalty term. *Inverse Problems*, 24(5):055020, 2008.

- [17] M. Grasmair, O. Scherzer, and M. Haltmeier. Necessary and sufficient conditions for linear convergence of l_1 -regularization. *Communications on Pure and Applied Mathematics*, 64(2):161–182, 2011.
- [18] H. Hallez, B. Vanrumste, R. Grech, J. Muscat, W. D. Clercq, A. Vergult, Y. D’Asseler, K. Camilleri, S. G. Fabri, S. V. Huffel, and I. Lemahieu. Review on solving the forward problem in EEG source analysis. *Journal of NeuroEngineering and Rehabilitation*, 4(46), 2007.
- [19] M. Hanke and W. Rundell. On rational approximation methods for inverse source problems. *Inverse Problems and Imaging*, 5(1):185–202, 2011.
- [20] E. Herman, A. Alexanderian, and A. K. Saibaba. Randomization and reweighted ℓ_1 -minimization for A-optimal design of linear inverse problems. *SIAM Journal on Scientific Computing*, 42(3):A1714–A1740, 2020.
- [21] F. Hettlich and W. Rundell. Iterative methods for the reconstruction of an inverse potential problem. *Inverse Problems*, 12:251–266, 1996.
- [22] M. Hinze, B. Hofmann, and T. N. T. Quyen. A regularization approach for an inverse source problem in elliptic systems from single Cauchy data. *Numerical Functional Analysis and Optimization*, 40(9):1080–1112, 2019.
- [23] V. Isakov. *Inverse Problems for Partial Differential Equations*. Springer-Verlag, 2005.
- [24] W. Jeong, S. Pyun, W. Son, and D. J. Min. A numerical study of simultaneous-source full waveform inversion with l_1 -norm. *Geophysical Journal International*, 194(3):1727–1737, 2013.
- [25] K. Kunisch and X. Pan. Estimation of interfaces from boundary measurements. *SIAM J. Control Optim.*, 32(6):1643–1674, 1994.
- [26] C. Li and G. Stadler. Sparse solutions in optimal control of PDEs with uncertain parameters: The linear case. *SIAM Journal on Control and Optimization*, 57(1):633–658, 2019.
- [27] D. A. Lorenz. Convergence rates and source conditions for Tikhonov regularization with sparsity constraints. *Journal of Inverse and Ill-posed Problems*, 16(5):463–478, 2008.
- [28] I. Loris, G. Nolet, I. Daubechies, and F. Dahlen. Tomographic inversion using ℓ_1 -norm regularization of wavelet coefficients. *Geophysical Journal International*, 170(1):359–370, 2007.
- [29] M. C. MacLachlan, J. Sundnes, and G. Lines. Simulation of ST segment changes during subendocardial ischemia using a realistic 3-D cardiac geometry. *IEEE Transactions on Biomedical Engineering*, 52(5):799–807, 2005.

- [30] B. F. Nielsen, M. Lysaker, and P. Grøttum. Computing ischemic regions in the heart with the bidomain model; first steps towards validation. *IEEE Transactions on Medical Imaging*, 32(6):1085–1096, 2013.
- [31] W. Ring. Identification of a core from boundary data. *SIAM Journal on Applied Mathematics*, 55(3):677–706, 1995.
- [32] J. Sarvas. Basic mathematical and electromagnetic concepts of the bio-magnetic inverse problem. *Physics in Medicine and Biology*, 32(1):11–22, 1987.
- [33] S. J. Song and J. G. Huang. Solving an inverse problem from bioluminescence tomography by minimizing an energy-like functional. *J. Comput. Anal. Appl.*, 14:544–558, 2012.
- [34] D. Wang, R. M. Kirby, R. S. MacLeod, and C. R. Johnson. Inverse electrocardiographic source localization of ischemia: An optimization framework and finite element solution. *Journal of Computational Physics*, (250):403–424, 2013.
- [35] L. Wang. *Applications of Sparse Regularization to Inverse Problem of Electrocardiography*. PhD thesis, 2012.
- [36] C. Wolters, A. Anwander, X. Tricoche, D. Weinstein, M. Koch, and R. MacLeod. Influence of tissue conductivity anisotropy on EEG/MEG field and return current computation in a realistic head model: a simulation and visualization study using high-resolution finite element modeling. *NeuroImage*, 30(3):813–826, 2006.
- [37] X. Xiang and H. Sun. Sparse reconstructions of acoustic source for inverse scattering problems in measure space. *Inverse Problems*, 36(3), 2020.